CHALMERS
UNIVERSITY OF TECHNOLOGY

Fast and Accurate Non-linear Model for Synchronous Machines Including Core Losses

Downloaded from: https://research.chalmers.se, 2026-09-14 21:29 UTC

Citation for the original published paper (version of record):
Abbas, A., Vesa, J., Khan, H. et al (2024). Fast and Accurate Non-linear Model for Synchronous Machines Including Core Losses. IEEE Transactions on Energy Conversion, 39(4): 2559-2567. http://dx.doi.org/10.1109/TEC.2024.3394612

N.B. When citing this work, cite the original published paper.

© 2024 IEEE. Personal use of this material is permitted. Permission from IEEE must be obtained for all other uses, in any current or future media, including reprinting/republishing this material for advertising or promotional purposes, or reuse of any copyrighted component of this work in other works.

(article starts on next page)

Fast and Accurate Non-Linear Model for Synchronous Machines Including Core Losses

Amr A. Abbas, *Graduate Student Member, IEEE*, Joonas Vesa, Hadhiq Khan, *Member, IEEE*, Hao Chen, Yujing Liu, *Senior Member, IEEE*, and Paavo Rasilo, *Member, IEEE*

***Abstract*—This paper presents a fast and accurate state-space model for synchronous machines taking into consideration the machine geometry, material non-linearities and core losses. The model is first constructed by storing the solutions of multiple static finite element (FE) simulations into lookup-tables (LUTs) to express the stator flux linkages as functions of the state variables, i.e., the winding currents and the rotor position. Different approaches are discussed to include the core loss into the model. A novel approach is presented for constructing a pre-computed LUT for the core loss as a function of the state variables and their time derivatives so that the loss can be directly interpolated when time-stepping the state-space model. The Simulink implementation of the proposed core-loss model shows a good match with time-stepping FE results with a 120-fold speedup in computation. In addition, comparison against calorimetric loss measurements for a 150-kVA machine operating under both sinusoidal and pulse-width modulated voltage supplies is presented to validate the model accuracy.**

***Index Terms*—Core loss, lookup-tables, state-space model, synchronous machine.**

I. Introduction

FAST and accurate models for electrical machines are indispensable, especially when an iterative controller design and validation process is involved or conducting a long drive-cycle simulation is required. For example, in the electric vehicle drive-cycle simulation, it is required to run the motor for around 10 to 30 minutes [1]. For such long simulations, the model has to be fast enough, and at the same time, sufficiently accurate [2].

Manuscript received 29 September 2023; revised 25 January 2024 and 21 March 2024; accepted 14 April 2024. Date of publication 29 April 2024; date of current version 26 November 2024. This work was supported in part by the European Union's Horizon 2021 under Grant 101056857 and in part by the Research Council of Finland under Grant 346440. Paper no. TEC-01124-2023. *(Corresponding author: Amr A. Abbas.)*

Amr A. Abbas is with the Electrical Engineering Unit, Tampere University, FI-33720 Tampere, Finland, and also with the Electrical Power Department, Faculty of Engineering, Cairo University, Giza EG-12613, Egypt (e-mail: amr.abbas@tuni.fi).

Joonas Vesa, Hadhiq Khan, and Paavo Rasilo are with the Electrical Engineering Unit, Tampere University, FI-33720 Tampere, Finland (e-mail: joonas.vesa@tuni.fi; hadhiq.khan@tuni.fi; paavo.rasilo@tuni.fi).

Hao Chen was with the Department of Electrical Engineering, Chalmers University of Technology, 41296 Gothenburg, Sweden. He is now with the College of Electrical Engineering, Zhejiang University, Hangzhou 310027, China (e-mail: hao.chen-ee@zju.edu.cn).

Yujing Liu is with the Department of Electrical Engineering, Chalmers University of Technology, SE-41296 Göteborg, Sweden (e-mail: yujing.liu@chalmers.se).

Color versions of one or more figures in this article are available at https://doi.org/10.1109/TEC.2024.3394612.

Digital Object Identifier 10.1109/TEC.2024.3394612

There are many techniques in the literature for motor modeling. The conventional dq0 model with constant inductances is a good choice for machine modeling from the computation time point of view. However, it ignores the effects of geometrical structures (i.e. stator slotting and rotor core shape), material non-linearities and losses, which leads to inaccuracies in the results [3], [4], [5]. There are some extensions for the model to include these non-idealities, but such models are no longer simple and need a lot of time to be constructed [6], [7], [8]. On the other hand, finite element (FE) models yield highly accurate results taking into consideration geometrical effects and material non-linearities. However, these models are very time consuming and not feasible for long simulations.

FE based state-space models are a good choice to simulate the synchronous machine in the time domain. These models are based on solving multiple static FE simulations and using these results to build lookup-tables (LUTs) to replace an analytical machine model. As these LUTs are based on FE solutions, they can yield accuracy comparable to FE simulations with shorter computation time.

The FE based state-space models can be divided into two categories based on how the model is developed. The first category uses the machine inductances to construct the LUTs. The authors in [3] build the model by storing the winding inductance matrix as a function of rotor position only, neglecting the saturation effects. A similar procedure is followed in [9] where the inductance and torque matrices are stored as functions of the rotor angle and stator currents. It has been reported in the literature that constructing the inductance matrix is a time consuming process and needs a large number of LUTs [4], [10].

The second category directly uses the current vs. flux-linkage relationship instead of machine inductances. In [4], the stator flux linkages are stored as functions of the stator currents and rotor position taking into consideration material non-linearity. The same approach is followed in [10] to build the flux-linkage LUTs for a synchronous generator using the stator current space vector instead of the actual phase currents to reduce the LUT size. However, the authors assume that the generator operates only in the third quadrant which does not fully represent the whole operating range of the machine. The authors in [11] propose using a state-space model where the stator currents are stored as functions of the stator flux linkages.

© 2024 The Authors. This work is licensed under a Creative Commons Attribution 4.0 License. For more information, see https://creativecommons.org/licenses/by/4.0/

In the aforementioned works, the state-space models are built without considering the machine core loss. Accurate computation of the core loss requires the transient flux-density distribution in the core, whose computation is very time consuming when transient FE simulations are used [12], [13].

Many attempts have been discussed in the literature to include the core-loss calculation in the state-space models. In [7], the core loss is included based on the open-circuit and short-circuit tests, and the loss at any other operation point is estimated from an analytical formula. However, the employed loss model considers only for the fundamental component of the loss due to its reliance on the Steinmetz formula. The authors in [14] represent the core loss with a parallel resistance as a LUT in the equivalent circuit. However, the evaluation of the resistance values is based on directly storing measured data into a LUT, and specific iron-loss models are not discussed. Additionally, the validation of the model is limited to the no-load condition. The work in [15] follows the same procedure, and the machine model including core loss is implemented into a real-time FPGA simulator. In [16], the core loss is included in the state-space model by considering the actual flux-density distribution in the core which was resolved with FE analysis. However, only the eddy current loss is included with the assumption of quadratic dependency on the time derivative of the flux density. This approach is not applicable to general non-linear power loss models.

In this paper, a non-linear state-space model for synchronous machines is built using the winding currents and rotor position as the state variables. This model will be called current based state-space model (CBSSM) for the rest of the paper. A new approach is proposed for efficiently including general post-processing core-loss models into the CBSSM. The approach is suitable for any non-linear iron-loss model where the instantaneous loss density can be expressed as a function of the flux density and its time derivative. One of such expressions is identified against iron-loss data produced with a 1-D numerical model of the hysteresis, eddy-current and excess losses in a single core lamination. The core-loss density in the FE integration points is then pre-calculated as a function of the state variables and their time derivatives. Pre-computed integrals of the loss density over the core volume are stored in LUTs to allow efficient and fast evaluation of the core loss during the transient simulation. The model is implemented in MATLAB / Simulink and verified against both time-stepping FE simulations and calorimetric core-loss measurements.

This paper is organized as follows: Subsection II-A describes the state-space model derivation. Subsection II-B explains the employed core-loss model, while Subsection II-C illustrates the identification process for the model parameters. Subsection II-D discusses three different implementation approaches for the loss model in Simulink. Section III validates the proposed core-loss model against the FE model and the measurements under grid supply and inverter supply with 1-kHz and 6-kHz switching frequencies. Finally, Section IV concludes the main points of the paper.

II. Methods

A. State-Space Model

The phase voltage equations of a three-phase synchronous machine are given by

$$\boldsymbol{u}_{\mathrm{abc}} = R_{\mathrm{s}}\boldsymbol{i}_{\mathrm{abc}} + \frac{d\boldsymbol{\psi}_{\mathrm{abc}}\left(\boldsymbol{i}_{\mathrm{abc(f)}}, \alpha\right)}{dt}, \tag{1}$$

where $\boldsymbol{u}_{\mathrm{abc}}$ and $\boldsymbol{\psi}_{\mathrm{abc}}$ are column vectors containing the stator phase voltages and flux linkages, respectively, $\boldsymbol{i}_{\mathrm{abc(f)}}$ contains the phase currents and possibly the field current in case of a wound-field machine, R_{s} is the stator phase resistance and α is the electrical rotor position angle. In this paper, we focus on a wound-field synchronous machine which is excited with constant field current, so that $di_{\mathrm{f}}/dt = 0$. The field current dependency is thus neglected from the following derivations for brevity. In the isolated star connection, the sum of the three phase currents is zero. This can be formulated in a matrix form as

$$\boldsymbol{i}_{\mathrm{abc}} = \boldsymbol{K}^{\mathrm{T}}\boldsymbol{i}_{\mathrm{ab}}, \quad \boldsymbol{K}\boldsymbol{u}_{\mathrm{abc}} = \boldsymbol{Q}\boldsymbol{U}_{123}, \tag{2}$$

where $\boldsymbol{U}_{123}$ contains the line-to-line voltages and $\boldsymbol{K}$ and $\boldsymbol{Q}$ are connection matrices [17] given by

$$\boldsymbol{Q} = \begin{bmatrix} 0 & 0 & -1 \\ -1 & 0 & -1 \end{bmatrix}, \quad \boldsymbol{K} = \begin{bmatrix} 1 & 0 & -1 \\ 0 & 1 & -1 \end{bmatrix}. \tag{3}$$

The electromagnetic torque τ and the phase flux linkages are calculated with a 2-D static FE solver as functions of stator currents and rotor position, and stored in LUTs. The time derivative of the flux linkage can be expressed as a function of the model state variables using the chain rule as

$$\frac{d\boldsymbol{\psi}_{\mathrm{abc}}}{dt} = \frac{\partial\boldsymbol{\psi}_{\mathrm{abc}}}{\partial\boldsymbol{i}_{\mathrm{ab(f)}}}\frac{d\boldsymbol{i}_{\mathrm{ab(f)}}}{dt} + \frac{\partial\boldsymbol{\psi}_{\mathrm{abc}}}{\partial\alpha}\omega, \tag{4}$$

where $\omega = d\alpha/dt$ is the rotor electrical speed. The partial derivatives in (4) are calculated by differentiating the phase flux-linkage LUTs obtained from the static FE simulation with respect to the state variables.

Substituting (4) into (1) using (2) and (3) leads to the state-space form of the stator currents as

$$\frac{d\boldsymbol{i}_{\mathrm{ab}}}{dt} = \left(\frac{\partial(\boldsymbol{K}\boldsymbol{\psi}_{\mathrm{abc}})}{\partial\boldsymbol{i}_{\mathrm{ab}}}\right)^{-1}\left[\boldsymbol{Q}\boldsymbol{U}_{123} - R_{\mathrm{s}}\boldsymbol{K}\boldsymbol{K}^{\mathrm{T}}\boldsymbol{i}_{\mathrm{ab}} - \boldsymbol{K}\frac{\partial(\boldsymbol{K}\boldsymbol{\psi}_{\mathrm{abc}})}{\partial\alpha}\omega\right]. \tag{5}$$

The matrix $\boldsymbol{K}$ in (5) is multiplied into the flux-linkage vector before the differentiation to reduce the number of the required LUTs.

The partial derivatives of the phase flux linkages with respect to the phase currents in (5) can be expressed using the stator current space vector. By knowing the following relationships

$$\boldsymbol{i}_{\alpha\beta} = \boldsymbol{T}\boldsymbol{i}_{\mathrm{abc}} = \boldsymbol{T}\boldsymbol{K}^{\mathrm{T}}\boldsymbol{i}_{\mathrm{ab}}, \tag{6a}$$

$$I^2 = \left\|\boldsymbol{i}_{\alpha\beta}\right\|^2, \tag{6b}$$

$$\tan\theta = \frac{i_{\beta}}{i_{\alpha}}, \tag{6c}$$

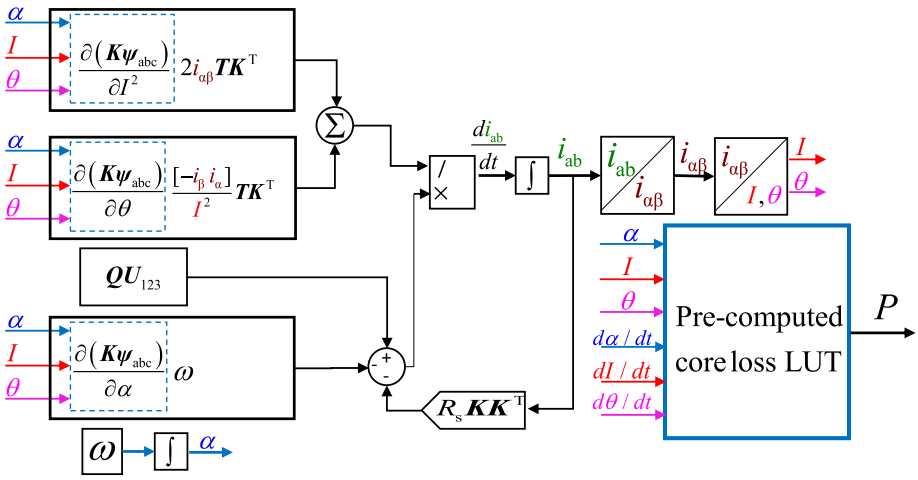

Fig. 1. State-space model block diagram with the pre-computed core-loss LUT (Approach 3 described in Section II-D).

where $\boldsymbol{i}_{\alpha\beta}$ contains the α and β components of the current space vector in the stator frame of reference, $\boldsymbol{T}$ is the Clarke transformation matrix

$$\boldsymbol{T} = \frac{2}{3}\begin{bmatrix} 1 & \frac{-1}{2} & \frac{-1}{2} \\ 0 & \frac{\sqrt{3}}{2} & \frac{-\sqrt{3}}{2} \end{bmatrix}, \tag{7}$$

and I and θ are the current space vector magnitude and angle, the first term in (5) can be written as

$$\frac{\partial(\boldsymbol{K}\boldsymbol{\psi}_{\text{abc}})}{\partial \boldsymbol{i}_{\text{ab}}} = \left[\frac{\partial(\boldsymbol{K}\boldsymbol{\psi}_{\text{abc}})}{\partial I^2}\frac{dI^2}{d\boldsymbol{i}_{\alpha\beta}} + \frac{\partial(\boldsymbol{K}\boldsymbol{\psi}_{\text{abc}})}{\partial\theta}\frac{d\theta}{d\boldsymbol{i}_{\alpha\beta}}\right]\frac{d\boldsymbol{i}_{\alpha\beta}}{d\boldsymbol{i}_{\text{ab}}}, \tag{8}$$

where

$$\frac{dI^2}{d\boldsymbol{i}_{\alpha\beta}} = 2\boldsymbol{i}_{\alpha\beta}^{\text{T}} \quad \text{and} \quad \frac{d\theta}{d\boldsymbol{i}_{\alpha\beta}} = \frac{[-i_\beta \;\; i_\alpha]}{I^2}. \tag{9}$$

Fig. 1 shows the block diagram of the state-space model which will be implemented in Simulink.

B. Core-Loss Model

Core-loss models similar to those discussed in [18] and [19] are considered. These models express the power loss density p in a core lamination as a function of the flux density vector $\boldsymbol{B}$ and its time derivative as $p(\boldsymbol{B}, \partial\boldsymbol{B}/\partial t)$. Examples of such models are the so-called loss-surface model [18] and the homogenized dynamic lamination model [19].

A modified version of the model in [19] is used to express the irreversible magnetic field $\boldsymbol{H}_{\text{irr}}$ as a function of $\boldsymbol{B}$ and $\partial\boldsymbol{B}/\partial t$ as

$$\boldsymbol{H}_{\text{irr}}\left(\boldsymbol{B}, \frac{\partial\boldsymbol{B}}{\partial t}\right) = p_1\left(1 + \frac{p_2}{\sqrt{p_3^2 + \left\|\frac{\partial\boldsymbol{B}}{\partial t}\right\|^2}}\right)\|\boldsymbol{B}\|^{p_4}\frac{\partial\boldsymbol{B}}{\partial t}, \tag{10}$$

where p_k are material parameters to be identified. The instantaneous core-loss density can then be calculated as

$$p\left(\boldsymbol{B}, \frac{\partial\boldsymbol{B}}{\partial t}\right) = \boldsymbol{H}_{\text{irr}}\left(\boldsymbol{B}, \frac{\partial\boldsymbol{B}}{\partial t}\right)\cdot\frac{\partial\boldsymbol{B}}{\partial t}. \tag{11}$$

A separate LUT for the $\boldsymbol{B}$ distribution is built while running the static FE solver. This LUT contains the flux-density vector $\boldsymbol{B}_i$ in all FE integration points i at each value of the state variables. By knowing $\boldsymbol{B}_i$ and $\partial\boldsymbol{B}_i/\partial t$ in the FE integration points of the core region Ω, the total core loss is obtained as

$$P = \int_\Omega p\left(\boldsymbol{B}, \frac{\partial\boldsymbol{B}}{\partial t}\right)d\Omega = \sum_i w_i p\left(\boldsymbol{B}_i, \frac{\partial\boldsymbol{B}_i}{\partial t}\right), \tag{12}$$

where i sums over the FE integration points and w_i are the integration weights. In this paper, the iron-loss model is evaluated *a posteriori* and $\boldsymbol{H}_{\text{irr}}$ is not included in the field solution.

Since the flux density distribution in the core is a function of the state variables, $\boldsymbol{B}_i(\boldsymbol{i}_{\text{ab(f)}}, \alpha)$, its time derivative can be expressed as

$$\frac{\partial\boldsymbol{B}_i}{\partial t} = \frac{\partial\boldsymbol{B}_i}{\partial\boldsymbol{i}_{\text{ab(f)}}}\frac{d\boldsymbol{i}_{\text{ab(f)}}}{dt} + \frac{\partial\boldsymbol{B}_i}{\partial\alpha}\omega. \tag{13}$$

Similar to (8), (13) can be re-written in terms of I, θ and α using the chain rule as

$$\frac{\partial\boldsymbol{B}_i}{\partial t} = \left(\frac{\partial\boldsymbol{B}_i}{\partial I^2}\frac{dI^2}{d\boldsymbol{i}_{\alpha\beta}} + \frac{\partial\boldsymbol{B}_i}{\partial\theta}\frac{d\theta}{d\boldsymbol{i}_{\alpha\beta}}\right)\boldsymbol{T}\boldsymbol{K}^{\text{T}}\frac{d\boldsymbol{i}_{\text{ab}}}{dt} + \frac{\partial\boldsymbol{B}_i}{\partial\alpha}\omega. \tag{14}$$

C. Core-Loss Model Parameter Identification

Parameters p_k are identified using the dynamic 1-D lamination model presented in [20]. Only the static major hysteresis loop, electrical conductivity and excess-loss coefficient are needed as inputs to the 1-D model. A brief description of this model is presented here.

By placing an infinitely large lamination with thickness d parallel to the xy-plane, the 1-D diffusion equation can be

written as

$$\frac{\partial^2 h(z,t)}{\partial z^2} = \sigma \frac{\partial b(z,t)}{\partial t}, \tag{15}$$

where σ is the electrical conductivity, and h and b are the field strength and flux density, respectively. The solution of this equation can be written as a cosine Fourier series expansion of the flux density with N_b terms

$$b(z,t) = \sum_{n=0}^{N_\mathrm{b}-1} b_n(t) \cos\left(\frac{2\pi n z}{d}\right). \tag{16}$$

The magnetic field strength is approximated in the same manner using a series expansion, ensuring that (15) is exactly satisfied. Due to the finite number of terms employed in the approximation, material properties are satisfied only in a weak sense by enforcing the orthogonality of the error between the approximated field strength and the actual field strength with respect to the cosine functions. This weak formulation leads to the following system of equations for the surface field strength h_s:

$$\begin{bmatrix} h_\mathrm{s}(t) \\ 0 \\ \vdots \end{bmatrix} = \frac{1}{d} \int_{-d/2}^{d/2} h(b(z,t)) \begin{bmatrix} \alpha_0(z) \\ \alpha_1(z) \\ \vdots \end{bmatrix} dz + \sigma d^2 \boldsymbol{C} \frac{d}{dt} \begin{bmatrix} b_0(t) \\ b_1(t) \\ \vdots \end{bmatrix} \tag{17}$$

where $\boldsymbol{C}$ is a constant matrix.

For a known average flux density $b_0(t)$, the system in (17) can be used to solve for the flux density distribution $b(z,t)$ and surface field $h_\mathrm{s}(t)$. The constitutive law comprises a static hysteretic relationship and an excess-loss contribution and is written as

$$h(b) = h_\mathrm{hy}(b) + c_\mathrm{ex} \left|\frac{\partial b}{\partial t}\right|^{-0.5} \frac{\partial b}{\partial t} \tag{18}$$

where c_ex is the excess loss coefficient.

The local magnetization power and the eddy-current and excess loss densities are obtained as

$$\begin{aligned} p_\mathrm{hy}(z,t) &= h_\mathrm{hy} \frac{\partial b(z,t)}{\partial t} \\ p_\mathrm{cl}(z,t) &= \sigma d^2 \sum_{m=0}^{N_\mathrm{b}-1} \sum_{n=0}^{N_\mathrm{b}-1} C_{mn} \frac{db_m(t)}{dt} \frac{db_n(t)}{dt} \\ p_\mathrm{ex}(z,t) &= c_\mathrm{ex} \left|\frac{\partial b(z,t)}{\partial t}\right|^{1.5}. \end{aligned} \tag{19}$$

By averaging (19) over the lamination thickness and the fundamental period in steady state, the total average iron-loss density can be calculated. The densities simulated at different excitations $b_0(t)$ can then be compared against the analytical expression (10) and (11) to identify the parameters p_k.

The loss model is identified for M600-50 A electrical steel sheets. The static hysteresis loops are measured with a standard Epstein frame setup with 300 mm × 30 mm samples and a DC hysteresisgraph. The lamination conductivity is 3 MS/m and the excess loss coefficient is 0.718 W/m^3(s/T)$^{1.5}$ [21]. Loss data is produced for sinusoidally varying average flux densities with amplitudes of 0.1... 2 T and frequencies of 50... 2000 Hz. The parameters p_k are then identified by fitting the analytical model (10)–(11) against this loss data using the non-linear least squares method. A comparison between the simulated and fitted losses is shown Fig. 2. The values of the fitted p_k parameters are presented in Table I.

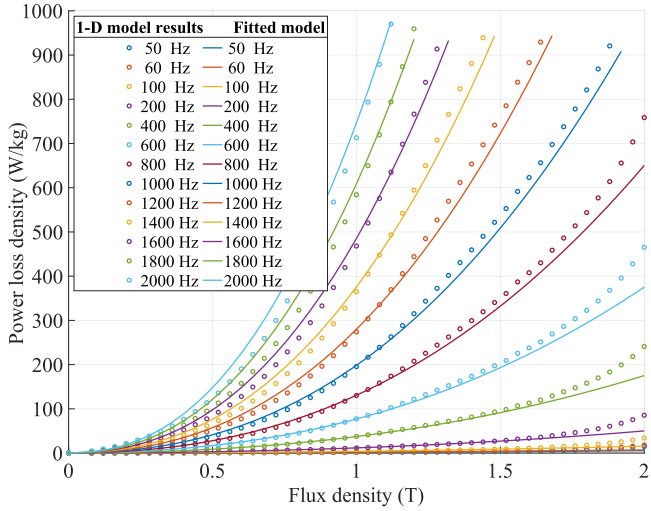

Fig. 2. Comparison of power loss density obtained from the dynamic 1-D lamination model and fitting parameters p_k.

TABLE I
IDENTIFIED p_k PARAMETERS

p_1 (A·m^{-1}T$^{-(p_4+1)}$Hz^{-1})	p_2 (T·Hz)	p_3 (T·Hz)	p_4
3.482×10^{-6}	2.436	0.164	0.422

D. Simulink Implementation

In order to include the core loss in the CBSSM, three different approaches are introduced to implement the loss model (12) into Simulink. Approach 1 is to implement the loss model (10) and the numerical integration (12) in Simulink using the built-in blocks. The time derivative of the flux density is calculated using (14). This requires to pre-compute and store the derivatives of $\boldsymbol{B}_i$ with respect to I, θ and α. The drawback of this approach is that the computational burden of the interpolations is large as it needs to interpolate for $\boldsymbol{B}_i$ and its partial derivatives $\partial \boldsymbol{B}_i/\partial I^2$, $\partial \boldsymbol{B}_i/\partial\theta$ and $\partial \boldsymbol{B}_i/\partial\alpha$ for all integration points i.

Approach 2 is similar to the previous one with the exception that the time derivative of the flux density is obtained by numerical differentiation using the built-in time-derivative block in Simulink. This approach interpolates only the flux-density data $\boldsymbol{B}_i$, which makes it faster than Approach 1.

Approach 3, which is the main contribution of this paper, is to pre-calculate the loss and store it in a separate LUT as shown in Fig. 1. Equation (12) shows that the core loss can be written

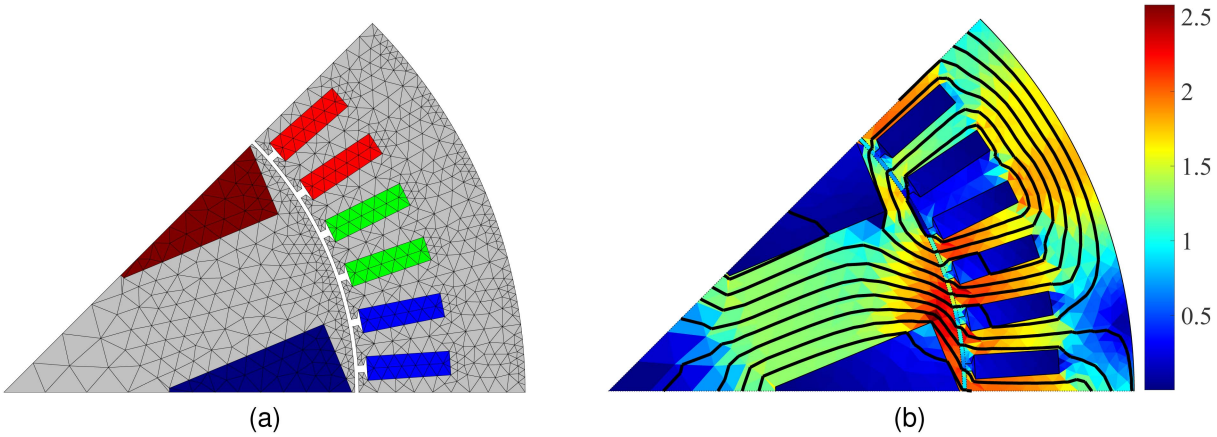

Fig. 3. Finite element model of the 200-kW machine. (a) FE mesh of 1/8 segment of the machine with 1476 elements and 871 nodes. (b) Flux-density distribution (T) of the machine.

TABLE II
PARAMETERS OF THE MACHINE UNDER STUDY

Parameter	Value
Rated shaft power	200 kW
Rated voltage	537 V
Rated frequency	200 Hz
Rated current	255 A
Number of poles	8
Number of slots	48

as a function of the state variables and their time derivatives as

$$P = f\left(I, \theta, \alpha, \frac{dI}{dt}, \frac{d\theta}{dt}, \omega\right), \tag{20}$$

implying that P can be pre-calculated and expressed as a LUT of six independent variables. The integration over Ω in (12) is computed in the pre-processing stage. The values of I, θ and α are the same as the values used to build LUTs of the state-space model. In addition, the values of their time derivatives are chosen so that they cover the entire operating range. In this case, (20) can be directly applied during the solution of the state-space model (5) as a separate LUT with minimal effect on the simulation time.

III. APPLICATION AND RESULTS

A. FE Validation and Computational Performance

The CBSSM model is first verified against a 2-D time-stepping FE simulation in case of a 200-kW wound-field synchronous motor meant for electric vehicle application. The model is supplied with both sinusoidal and pulse-width modulated (PWM) voltage supplies and constant field current. In-house MATLAB-based FE solvers are used for the static and time-stepping simulations. Table II lists the parameters of the machine under study. The FE mesh of one symmetry sector of the machine is presented in Fig. 3(a). Fig. 3(b) illustrates the flux density distribution under rated conditions.

TABLE III
DISCRETIZATION OF VARIABLES FOR THE MACHINE MODEL LUTS

Quantity	Number of points	Range
α	85	$-\pi$ ... π rad
I	21	0 ... $3I_{\text{rated}}$
θ	37	$-\pi$ ... π rad

TABLE IV
COMPARISON OF THE CBSSM AND FE MODELS WITHOUT CORE-LOSS MODELS

Quantity	CBSSM	FE	Difference
RMS current (A)	252	252	~ 0
Average torque (Nm)	594	597	0.5%
Simulation time per time step (ms)	0.15	16	106-fold speed-up

TABLE V
DISCRETIZATION OF VARIABLES FOR THE CORE-LOSS MODEL

Quantity	Number of points	Range
ω	6	0 ... 1500 $\frac{\text{rad}}{\text{s}}$
$\frac{dI}{dt}$	15	-10^9 ... 10^9 $\frac{\text{A}}{\text{s}}$
$\frac{d\theta}{dt}$	13	-4000 ... 4000 $\frac{\text{rad}}{\text{s}}$

Table III shows the number of data points used to build the model LUTs using the static FE solver. The rotor electrical position angle discretization takes the form of $12k + 1$, where k is an integer and 12 is the number of slots per pole pair. The current range is chosen to surely cover all realistic operation points.

Fig. 4 compares the phase currents obtained from the CBSSM and FE models under sinusoidal (Fig. 4(a)) and PWM (b) voltage supplies. Fig. 4(c) shows the current harmonic spectrum comparison between the two models in case of PWM supply. Table IV compares the RMS current, average torque and average simulation time per time step for both models with no core-loss model implemented. It is obvious that the computation time is greatly reduced while the accuracy is maintained.

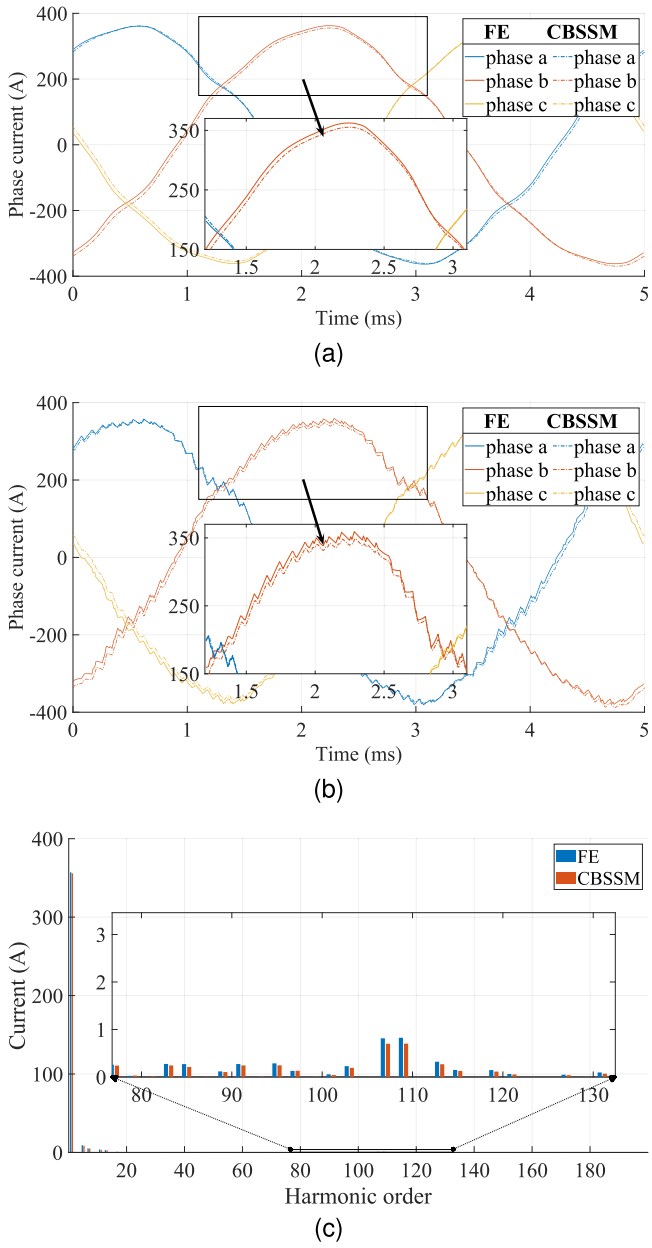

Fig. 4. Comparison of phase currents from the FE and CBSSM models with different voltage supplies. (a) Sinusoidal voltage supply. (b) PWM voltage supply (10 kHz switching frequency). (c) Current harmonic spectrum comparison at PWM supply.

Table V shows the number of data points used to discretize the state variables' time derivatives to pre-calculate the core loss according to (20). The ranges of these variables are obtained by running the model at different operating points under both sinusoidal and PWM supplies and observing the ranges of variation. It is worth noting that the number of static FE simulations needed to build up the LUTs for ψ, τ and $\boldsymbol{B}_i$ does not change from the values reported in Table III even if the discretization for the state variables' time derivatives is changed.

Table VI compares the different core-loss implementation approaches to the FE model with the sinusoidal and the PWM supplies. These results are obtained at the rated operating point

TABLE VI
COMPARISON BETWEEN THE FE MODEL AND THE CBSSM MODEL WITH DIFFERENT CORE-LOSS IMPLEMENTATION APPROACHES UNDER SINUSOIDAL AND PWM SUPPLIES

	Core-loss approaches	Approach 1	Approach 2	Approach 3	FE
Sinusoidal	Core loss (W)	915	970	963	1015
	Simulation time per time step (ms)	28	5	0.15	18
PWM	Core loss (W)	1438	1515	1515	1502
	Simulation time per time step (ms)	28	5	0.15	18

TABLE VII
PARAMETERS OF THE EXPERIMENTAL MACHINE

Parameter	Value
Rated electrical power	150 kVA
Rated voltage	400 V
Rated frequency	50 Hz
Rated current	217 A
Number of poles	4
Number of slots	48

of the machine. The table clearly shows the superiority of Approach 3 over the other approaches in terms of simulation time. For a simulation with 1000 time steps per fundamental period, it takes only 150 ms to simulate the full period. This is much less than the 18 seconds taken by the FE model. Comparison of the average simulation times per time step in Tables IV and VI shows that inclusion of the core loss using Approach 3 doesn't affect the computation time, which proves the advantage of the proposed method. In terms of speed, the proposed method is 120 times faster than the FE model and 185 and 33 times faster than Approaches 1 and 2, respectively.

Approaches 1 and 2 need to interpolate $\boldsymbol{B}_i$ for all integration points i, calculate its time derivative and then apply the loss model in (11), which makes them slower than the proposed approach (Approach 3). The accuracy of the proposed approach can be further increased by increasing the number of the state variables' time derivative points in the loss pre-computation stage.

B. Experimental Validation

To show that the chosen iron-loss model (10)-(11) is able to provide a realistic estimate of the losses, a comparison against calorimetric loss measurements of a 150-kVA wound-field synchronous machine is made under both sinusoidal and PWM supplies. The machine parameters and the FE mesh of one symmetry sector are shown in Table VII and Fig. 5, respectively. The measurement setup is described in [21] and [22]. The CBSSM is built for this machine following the same procedure as described in Subsection III-A.

The study is performed for PWM switching frequencies of 1-kHz and 6-kHz besides the grid supply. The losses are measured at electrical powers of 25%, 50%, 75% and 100% of the rated power with 0.8 capacitive displacement factor for each supply. Fig. 6 and Table VIII compare the simulated core losses

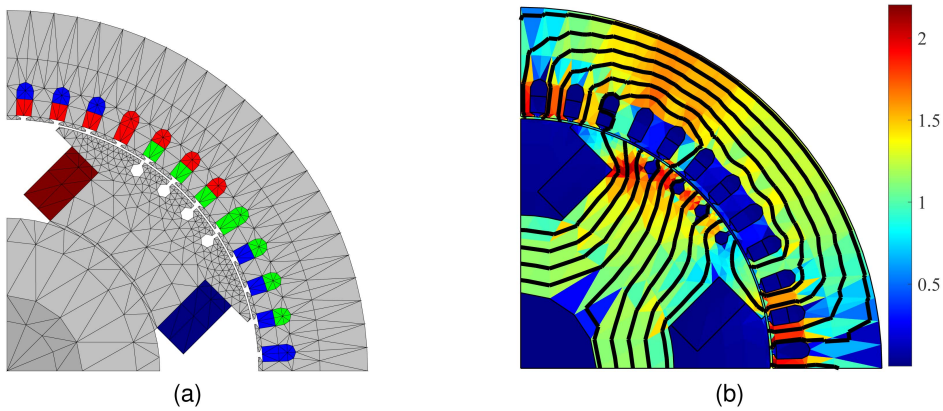

Fig. 5. Finite element model of the 150-kVA machine. (a) FE mesh of 1/4 segment of the machine with 1434 elements and 1024 nodes. (b) Flux-density distribution (T) of the machine.

TABLE VIII
NUMERICAL VALUES OF THE MEASURED AND SIMULATED CORE LOSS WITH DIFFERENT APPROACHES, AND ERROR LIMITS FOR THE MEASURED LOSS

Core loss (W)	Load %	Measurement	Approach 1	Approach 2	Approach 3	FE	FE with damper bars
Sinusoidal	25	1365 ± 103	1529	1571	1566	1562	1536
	50	1565 ± 114	1639	1676	1679	1667	1634
	75	1750 ± 140	1748	1789	1799	1764	1729
	100	2026 ± 196	1854	1890	1908	1872	1832
6 kHz	25	1840 ± 106	1940	1982	1980	1885	1974
	50	1948 ± 118	2077	2113	2157	2007	2057
	75	2139 ± 144	2188	2250	2237	2119	2146
	100	2383 ± 200	2441	2340	2292	2228	2240
1 kHz	25	2145 ± 108	1970	2011	2114	1979	2100
	50	2344 ± 122	2099	2137	2287	2112	2189
	75	2475 ± 152	2211	2252	2353	2234	2280
	100	2676 ± 213	2349	2359	2390	2340	2368

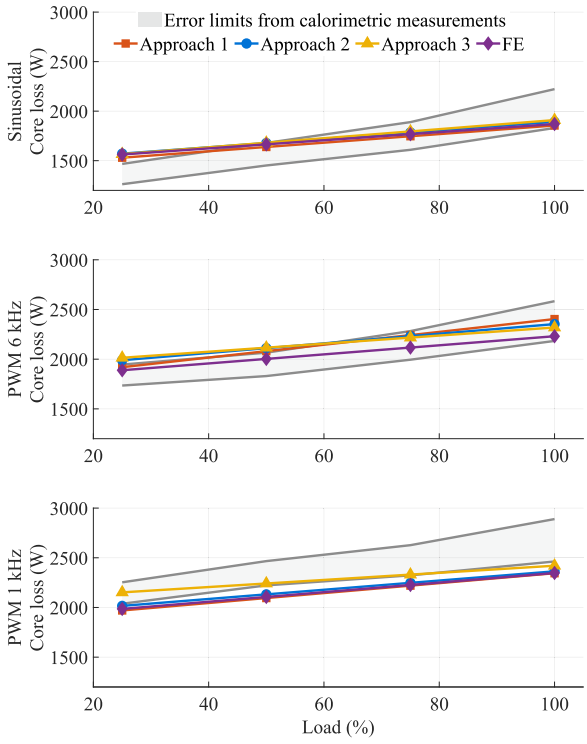

Fig. 6. Measured and simulated core loss with different approaches as a function of loading under different types of voltage supply.

against the measurements for different loadings. The gray area in the figure represents uncertainty range of the loss measured with the calorimetric setup [22].

For the sinusoidal supply, the results from the three approaches and the FE model align well with the measurements. The simulated results can be seen to be within the measurement limits. Changing to a PWM supply with 6 kHz switching frequency leads to increasing losses at various loading points compared to the sinusoidal supply case. Nevertheless, the simulated losses still comply well with the measured losses. Decreasing the switching frequency to 1 kHz leads to a more significant increase in core loss. Still, the simulated losses with the three approaches and the FE show good agreement.

It is worth mentioning that the machine is equipped with rotor damper bars, a skewed stator and conducting end-plates that are included in the measured losses but not taken into account in the Simulink models for this implementation, since the focus is on efficient implementation of the core-loss model. However, by performing another set of time-stepping FE simulations in which the damper winding was considered, it was confirmed that the effect of the damper winding on the iron loss itself is negligible. This can be seen by comparing the iron-loss values in the last two columns of Table VIII. The measurements are thus considered as a reasonable validation for the model.

IV. Conclusion

A finite element based state-space model for synchronous machines including core losses is developed and verified against a 2-D time-stepping FE model and calorimetric loss measurements. The instantaneous loss density is represented as a function of the flux density and its time derivative. Three different approaches for including core loss to the state-space model are discussed. The proposed approach based on pre-calculating and storing the core loss in a lookup table is shown to be 120 times faster than the FE calculations. The flux-density LUT construction from the static FE simulations remains unchanged even if the loss-model parameters are changed. Only the loss table (20) need to be recalculated if the parameters change. The simulated losses showed good correspondence with the calorimetric loss measurement of a 150-kVA synchronous machine under different voltage supplies.

This model can be best suited in detailed long driving-cycle simulations of traction applications where high fidelity models with computationally efficient calculations are essential for correct performance assessment. Moreover, the same implementation procedure can be extended for application in other magnetic devices such as transformers and inductors.

IV. Acknowledgment

Views and opinions expressed are however those of the author(s) only and do not necessarily reflect those of the European Union or the European Climate, Infrastructure and Environment Executive Agency (CINEA). Neither the European Union nor the granting authority can be held responsible for them.

References

[1] G. Amirjamshidi and M. J. Roorda, "Development of simulated driving cycles for light, medium, and heavy duty trucks: Case of the toronto waterfront area," *Transp. Res. Part D: Transport Environ.*, vol. 34, pp. 255–266, 2015.

[2] B. Dianati, S. Kahourzade, and A. Mahmoudi, "Optimization of axial-flux induction motors for the application of electric vehicles considering driving cycles," *IEEE Trans. Energy Convers*, vol. 35, no. 3, pp. 1522–1533, Sep. 2020.

[3] O. A. Mohammed, S. Liu, and Z. Liu, "Physical modeling of PM synchronous motors for integrated coupling with machine drives," *IEEE Trans. Magn.*, vol. 41, no. 5, pp. 1628–1631, May 2005.

[4] L. Quéval and H. Ohsaki, "Nonlinear abc-model for electrical machines using N-D lookup tables," *IEEE Trans. Energy Convers.*, vol. 30, no. 1, pp. 316–322, Mar. 2015.

[5] S. Kallio, J. Karttunen, M. Andriollo, P. Peltoniemi, and P. Silventoinen, "Finite element based phase-variable model in the analysis of double-star permanent magnet synchronous machines," in *Proc. Int. Symp. Power Electron. Power Electron., Elect. Drives, Automat. Motion*, 2012, pp. 1462–1467.

[6] D. E. Pinto, A.-C. Pop, J. Kempkes, and J. Gyselinck, "Dq0-modeling of interior permanent-magnet synchronous machines for high-fidelity model order reduction," in *Proc. Int. Conf. Optim. Elect. Electron. Equip., Int. Aegean Conf. Elect. Mach. Power Electron.*, 2017, pp. 357–363.

[7] X. Chen, J. Wang, B. Sen, P. Lazari, and T. Sun, "A high-fidelity and computationally efficient model for interior permanent-magnet machines considering the magnetic saturation, spatial harmonics, and iron loss effect," *IEEE Trans. Ind. Electron*, vol. 62, no. 7, pp. 4044–4055, Jul. 2015.

[8] S. Li, D. Han, and B. Sarlioglu, "Modeling of interior permanent magnet machine considering saturation, cross coupling, spatial harmonics, and temperature effects," *IEEE Trans. Transp. Electrific.*, vol. 3, no. 3, pp. 682–693, Sep. 2017.

[9] M. R. Raia, A.-C. Pop, and C. Martis, "Scalable abc-modelling of permanent magnet synchronous machines for model order reduction," in *Proc. IEEE Workshop Elect. Mach. Des., Control Diagnosis*, vol. 1, 2019, pp. 83–88.

[10] Q. H. Quadri, S. Nuzzo, M. Rashed, C. Gerada, and M. Galea, "Modeling of classical synchronous generators using size-efficient lookup tables with skewing effect," *IEEE Access*, vol. 7, pp. 174551–174561, 2019.

[11] P. Rasilo, M. A. Lemesle, A. Belahcen, A. Arkkio, and M. Hinkkanen, "Comparison of finite-element-based state-space models for PM synchronous machines," *IEEE Trans. Energy Convers.*, vol. 29, no. 2, pp. 535–543, Jun. 2014.

[12] M. Van der Geest, H. Polinder, and J. A. Ferreira, "Computationally efficient 3D fem rotor eddy-current loss calculation for permanent magnet synchronous machines," in *Proc. IEEE Int. Electric Mach. Drives Conf.*, 2015, pp. 1165–1169.

[13] P. Handgruber, A. Stermecki, O. Bíró, A. Belahcen, and E. Dlala, "Three-dimensional eddy-current analysis in steel laminations of electrical machines as a contribution for improved iron loss modeling," *IEEE Trans. Ind. Appl.*, vol. 49, no. 5, pp. 2044–2052, Sep.–Oct. 2013.

[14] S. Gradev and H.-G. Herzog, "Integration of iron-loss resistance into dynamic models of 2 × 3-phase hybrid-excited synchronous machine," *IEEE Trans. Energy Convers*, vol. 33, no. 4, pp. 1700–1711, Dec. 2018.

[15] R. Scheer, Y. Bergheim, D. Heintges, N. Rahner, R. Gries, and J. Andert, "An FPGA-based real-time spatial harmonics model of a PMSM considering iron losses and the thermal impact," *IEEE Trans. Transp. Electrific.*, vol. 8, no. 1, pp. 1289–1301, Mar. 2022.

[16] D. E. Pinto, A. C. Pop, J. Kempkes, and J. Gyselinck, "Reduced-order eddy-current loss modelling of electrical machines using lookup tables obtained via 2D finite-element," in *Proc. 13th Int. Conf. Elect. Mach.*, 2018, pp. 386–392.

[17] A. Arkkio, "Analysis of induction motors based on the numerical solution of the magnetic field and circuit equations," Ph.D. dissertation, Dept. Elect. Commun. Eng., Helsinki Univ. Technol., Espoo, Finland, 1987.

[18] A. T. Vo, M. Fassenet, V. Préault, C. Espanet, and A. Kedous-Lebouc, "New formulation of loss-surface model for accurate iron loss modeling at extreme flux density and flux variation: Experimental analysis and test on a high-speed PMSM," *J. Magn. Magn. Mater*, vol. 563, Dec. 2022, Art. no. 169935.

[19] F. Purnode, F. Henrotte, F. Caire, J. D. Silva, G. Louppe, and C. Geuzaine, "A material law based on neural networks and homogenization for the accurate finite element simulation of laminated ferromagnetic cores in the periodic regime," *IEEE Trans. Magn.*, vol. 58, no. 9, Sep. 2022, Art. no. 7500204.

[20] P. Rasilo, E. Dlala, K. Fonteyn, J. Pippuri, A. Belahcen, and A. Arkkio, "Model of laminated ferromagnetic cores for loss prediction in electrical machines," *IET Electric Power Appl.*, vol. 5, no. 7, pp. 580–588, Aug. 2011.

[21] P. Rasilo, A. Belahcen, and A. Arkkio, "Experimental determination and numerical evaluation of core losses in a 150-kVA wound-field synchronous machine," *IET Electric Power Appl.*, vol. 7, no. 2, pp. 97–105, 2013.

[22] P. Rasilo, J. Ekström, A. Haavisto, A. Belahcen, and A. Arkkio, "Calorimetric system for measurement of synchronous machine losses," *IET Electrific. Power Appl.*, vol. 6, no. 5, pp. 286–294, 2012.

Amr A. Abbas (Graduate Student Member, IEEE) received the B.Sc. and M.Sc. degrees from the Electrical Power and Machines Department, Cairo University, Giza, Egypt, in 2017 and 2021, respectively. Since 2022, he has been working toward the Ph.D. degree in electrical engineering with Tampere University, Tampere, Finland. His research interests include modeling of electrical machines, passive magnetic components and model order reduction.

Joonas Vesa received the B.Sc. and M.Sc. degrees in mathematics and the Ph.D. degree in computational electromagnetics from the Tampere University of Technology (currently Tampere University), Tampere, Finland, in 2014, 2016, and 2021, respectively Since 2022, he has been a Postdoctoral Researcher with the Group of Electromechanics, Tampere University, developing computational material models for soft magnetic composites.

Hadhiq Khan (Member, IEEE) received the B. Tech. and Ph.D. degrees in electrical engineering from the National Institute of Technology Srinagar, India, in 2015 and 2020, respectively. Since 2023, he has been a Postdoctoral Researcher with the Group of Electromechanics, Tampere University, Tampere, Finland. His research interests include model order reduction of circuits and systems, modelling and control of power train components, and power electronics.

Hao Chen received the B.Sc. degree in electrical engineering from the School of Electrical Engineering, Beijing Jiaotong University, Beijing, China, in 2012, and the Ph.D. degree in control science and engineering from the School of Automation, Beijing Institute of Technology, Beijing, China, in 2019. From 2016 to 2018, he was with the Department of Electrical and Computer Engineering, Marquette University, Milwaukee, WI, USA, as a Joint Ph.D. Student. From 2019 to 2021, he was a Postdoctoral Research Fellow with the School of Electrical and Electronic Engineering, Nanyang Technological University, Singapore. From 2022 to 2023, he was a Researcher with the Department of Electrical Engineering, Chalmers University of Technology, Gothenburg, Sweden. He is currently an Assistant Professor with the College of Electrical Engineering, Zhejiang University, Hangzhou, China. His research interests include the design and optimization of electric machines, power electronic drives, and motor control

Yujing Liu (Senior Member, IEEE) received B.Sc., M.Sc. and Ph.D. degrees in electrical engineering from Harbin Institute of Technology, Harbin, China, in 1982, 1985, and 1988, respectively. From 1996 to 2013, he was with ABB Corporate Research, Västerås, Sweden. Since 2013, he has been a Professor of electrical power engineering with the Chalmers University of Technology, Gothenburg, Sweden. His research interests include research on motors, converters, and wireless charging for electric vehicles, generators and power electronics for tidal power conversion, and high efficiency machines for energy saving in industrial applications. Yujing Liu is also the Member with Swedish Standard Committee on Electrical Machines.

Paavo Rasilo (Member, IEEE) received the M.Sc. (Tech.) degree from the Helsinki University of Technology (currently Aalto University), Espoo, Finland, in 2008 and the D.Sc. (Tech.) degree from Aalto University, Espoo, Finland, in 2012. He is currently an Associate Professor with the Electrical Engineering Unit, Tampere University, Tampere, Finland. His research interests include computational electromagnetics and magnetic material modeling related to electrical machines, passive magnetic components, wireless power transfer, and energy harvesting.